RSC Advances

PAPER

View Article Online
View Journal | View Issue

Cite this: *RSC Adv.*, 2024, **14**, 19257

Post-functionalization of triamino-phenazinium dyes to reach near-infrared emission†

Tatiana Munteanu, [a] Jean-François Longevial, [ab] Gabriel Canard, [a] Denis Jacquemin, [cd] Simon Pascal *[ac] and Olivier Siri *[a]

Received 2nd May 2024
Accepted 20th May 2024

DOI: 10.1039/d4ra03245d

rsc.li/rsc-advances

This study presents the synthesis and characterization of phenazinium dyes with absorption ranging from red to far-red, as well as emission extending into the far-red to near-infrared (NIR) region. The procedure involves the post-functionalization of a triamino-phenazinium that was recently reported as a theranostic agent. The introduction of electron-withdrawing moieties is accomplished through acylation or aromatic nucleophilic substitution. For one of the obtained products, a further substitution step could be achieved with primary amines to tune the electron density of the phenazinium core. The isolated dyes exhibit promising features that hold potential for future applications as biological markers or therapeutic agents.

Introduction

Following the serendipitous discovery of Mauveine by Perkin in 1856,[1] phenazine dyes have known a period of industrial blossoming, marking the transition from natural pigments to synthetic dyes due to advantageous scalable fabrication, faster dying processes, deep coloration of various substrates and high photostability.[2–4] Nowadays, the appealing features of phenazines and their cationic analogues, phenaziniums, have attracted the interest of researchers in a wide range of applications including the biomedical field. Indeed, this family of chromophores is displaying cytotoxicity through radical oxygen species generation, pH sensitivity, high Stokes shift and tunable photophysical properties, which are sought for optical bioimaging.[5,6]

Amino-phenazine and amino-phenazinium derivatives clearly stand out in terms of synthesis versatility and superior photophysical properties. Indeed, the amino moieties notably increase the electron density on the phenazine aromatic system and improve the fluorescence efficiency by suppressing non-radiative relaxation processes.[7] Classical examples that are worth mentioning are clofazimine and derived structures that were clinically tested as antituberculosis agents,[8–11] Safranin-O with remarkable photodynamic antimicrobial activity[12–14] and Neutral Red, which gave the name to the well-known Neutral Red uptake assay, providing a quantitative estimation of cell viability/cytotoxicity (Fig. 1).[15,16] Neutral Red has also been studied as a theranostic agent *in vitro*, however, *in vivo* testing is being limited by its absorption at high energy (λ_{abs} = 530 nm), which do not match the biological transparency window.[17,18]

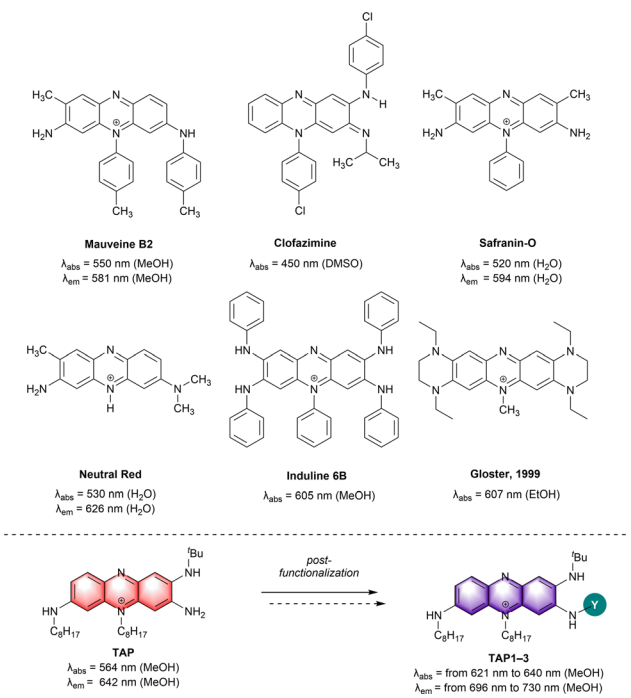

Fig. 1 Representative examples of amino-phenazine dyes (top) and amino-phenaziniums reported herein (bottom). Counterions omitted for clarity.

[a]*Aix Marseille Univ., CNRS UMR 7325 Centre Interdisciplinaire de Nanoscience de Marseille (CINaM), Campus de Luminy, 13288 Marseille cedex 09, France. E-mail: simon.pascal@cnrs.fr; olivier.siri@univ-amu.fr*

[b]*Université de Lorraine, LCP-A2MC, F-57000 Metz, France*

[c]*Nantes Université, CEISAM UMR 6230, CNRS, Nantes F-44000, France*

[d]*Institut Universitaire de France (IUF), Paris, France*

† Electronic supplementary information (ESI) available. CCDC 2339798. For ESI and crystallographic data in CIF or other electronic format see DOI: https://doi.org/10.1039/d4ra03245d

For bio-imaging and photodynamic therapy purposes, the increased availability of laser sources and of diagnostic tools pushes the research towards the development of far-red and near-infrared (NIR) dyes, offering superior efficiency in terms of imaging resolution and safer incident light, respectively.[19,20] Up to now, only few works report efficient strategies to redshift the optical properties of amino-phenazinium chromophores towards the NIR (Fig. 1). For instance, the extension and enrichment of the π-system of Induline 6B *via* the introduction of phenyl rings at the nitrogen atoms was a successful approach and resulted in a red located absorption maximum (λ_{abs} = 605 nm).[2] Notably, the rigidification of the chromophore core, a strategy extensively applied for the design of NIR dyes[21–25] was also tested in case of the phenazine derivatives. In a study described by Gloster and coworkers the incorporation of a peripheral tetrahydro-pyrazino moiety to the phenazine core led to a redshift of the absorption to a λ_{max} value of 607 nm *vs.* 564 nm for the non-rigidified congener. The induced restricted nitrogen atoms rotation eliminates the possibility of a twisted intramolecular charge transfer complex, improving also both the fluorescence and singlet oxygen quantum yields.[26] In 2015, the attachment of strong guanidino donors, known for their modulation of the HOMO–LUMO gap, has been reported by the group of Himmel.[7] Replacing classical amino functionalities by the guanidino groups provided a phenazine with strong orange-red emission (Φ = 0.39 at λ_{em} = 568 nm) and Stokes shift of up to 8750 cm^{-1} in H_2O.

More recently, we reported the remarkable theranostic potential of triamino-phenazinium **TAP** (Fig. 1), which is synthesized in few steps and that features strong red fluorescence, two-photon absorption in the NIR and singlet oxygen generation capabilities, along with a selectivity for mitochondria staining.[27] These unique assets prompted us to explore the possibility to tune the optical properties of **TAP** *via* straightforward modifications. We consequently report in this study the synthesis and photophysical characterization of a series of amino-phenazinium dyes, which show attractive optical features towards potent biological applications. The introduction of electron-withdrawing groups (EWG) on the available primary amine position has an impact on the structural and electrochemical properties of the dyes, but also resulted in a noticeable redshift of the absorption and emission bands towards the NIR domain, reaching wavelengths of interest corresponding to the biological transparency windows.[28]

Results and discussion

Synthesis

This work was initiated by considering the acylation of the primary amine function of **TAP**. Despite the limited nucleophilicity of the targeted amino group, which has a pronounced sp^2 character due to its involvement in the positive charge delocalization,[27] the acylation was envisaged using highly reactive and commercially available acyl chlorides or anhydrides (Scheme 1). Moreover, to overcome the acylation of the two secondary amines, high excess of the acylating reagents and elevated temperatures were avoided at first. The acylation of

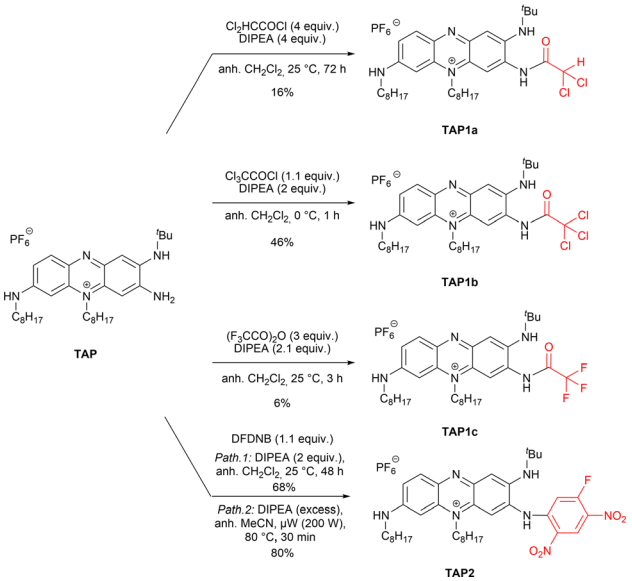

Scheme 1 Functionalization of **TAP** leading to **TAP1a–c** and **TAP2**.

TAP using dichloroacetyl chloride was achieved at room temperature, affording **TAP1a** as a blue dye. The yield was slightly enhanced from 9% to 16% when an excess of the reagent was used along with a prolonged reaction time, from 16 to 72 hours. To achieve the acylation with the more reactive trichloroacetyl chloride, the reaction mixture was kept at 0 °C, affording the derivative **TAP1b** in 46% yield in only 1 hour. Unfortunately, the reaction yield could not be increased neither using a reagent (trichloroacetyl chloride) excess nor with longer reaction times. It is worth to note that the fluorinated phenazinium **TAP1c** was particularly challenging to isolate and required careful handling to avoid a possible hydrolysis of amide function. Then, the reactivity of **TAP** regarding nucleophilic aromatic substitution was investigated using the commercial building block 1,5-difluoro-2,4-dinitrobenzene (DFDNB). Due to the presence of two nitro moieties in *para* position, the C–F bond in DFDNB is strongly polarized, turning it into an electrophilic reagent of choice. The resulting blue-colored dye **TAP2**, introducing a fluoro-dinitrophenyl moiety, was isolated in 68% yield after purification by column chromatography. This later yield could be significantly improved to 80% with shorter reaction time by using microwave irradiation.

Interestingly, the remaining electrophilic carbon on the highly electron-deficient fluoro-dinitrophenyl unit turns **TAP2** into a viable platform in a strategy meant to use **TAP2** for bioconjugation or attachment of other nucleophilic moieties for biological recognition. To confirm this hypothesis, we attempted to react **TAP2** with commercial *n*-butylamine and *p*-anisidine, yielding the desired products **TAP3a** and **TAP3b** as purple solids with excellent yields (Scheme 2). A similar reaction performed with *m*,*m*′-CF_3-aniline led to the recovery of the starting material, highlighting that such substitution was not possible with poorly nucleophilic amines.

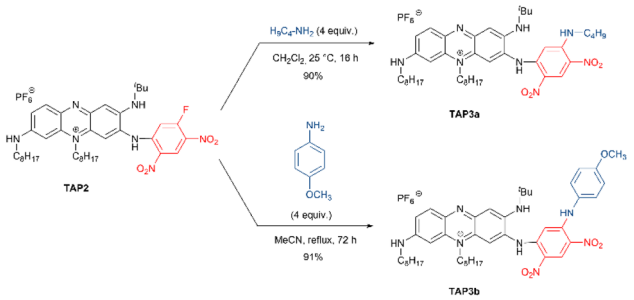

Scheme 2 Aromatic nucleophilic substitution performed on **TAP2** for the synthesis of dyes **TAP3a,b**.

Structural analysis

All functionalized phenaziniums were characterized through NMR and HRMS measurements, and their cationic nature was confirmed by the presence of the hexafluorophosphate counterion (see NMR spectra in Fig. S10–S29, ESI†). Additionally, single crystals of **TAP3a**, suitable for XRD analysis, were obtained by slow diffusion of pentane in a dichloromethane (DCM) solution of the compound. The X-ray structure depicted in Fig. 2 fully established the tricyclic and planar phenazinium core with a maximum deviation from planarity of 0.100 Å (for the N(2) atom). In contrast with the parent dye **TAP** where the positive charge is stabilized by delocalization involving the lone pair of N(4) (delocalization on the N(4)–C(4)–C(5)–C(6)–N(2) segment), the N(4) atom in **TAP3a** is strongly conjugated with the nitro function (sp^2 character). As a result, the positive charge is now stabilized by intramolecular delocalization involving N(5) over the N(2)–C(7)–C(8)–C(9)–N(5) unit. Moreover, we observe that the amino-dinitrophenyl substituent adopts a twisted position, at an angle of 72° in respect to the phenazinium plane, probably due to a simultaneous effect of steric hindrance and H-bond interactions.

Electrochemical properties

The parent phenazinium **TAP** as well as the modified dyes **TAP1–3** were investigated by cyclic voltammetry, to gain insights

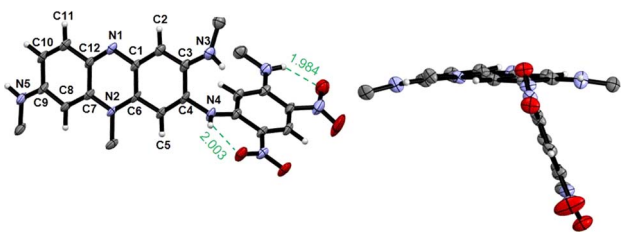

Fig. 2 ORTEP views of **TAP3a** (right: side view, left: top view). Alkyl chains and counterion PF_6^- omitted for clarity. Ellipsoids drawn at 50% probability. Selected bond lengths (Å): N(1)–C(1) 1.365(7), N(1)–C(12) 1.322(8), N(2)–C(6) 1.379(8), N(2)–C(7) 1.367(7), N(3)–C(3) 1.368(8), N(4)–C(4) 1.417(7), N(5)–C(9) 1.334(8), C(1)–C(2) 1.412(9), C(1)–C(6) 1.420(8), C(2)–C(3) 1.374(8), C(3)–C(4) 1.444(9), C(4)–C(5) 1.372(9), C(5)–C(6) 1.404(7), C(7)–C(8) 1.405(9), C(7)–C(12) 1.450(8), C(8)–C(9) 1.392(8), C(9)–C(10) 1.432(9), C(10)–C(11) 1.351(9), C(11)–C(12) 1.416(8).

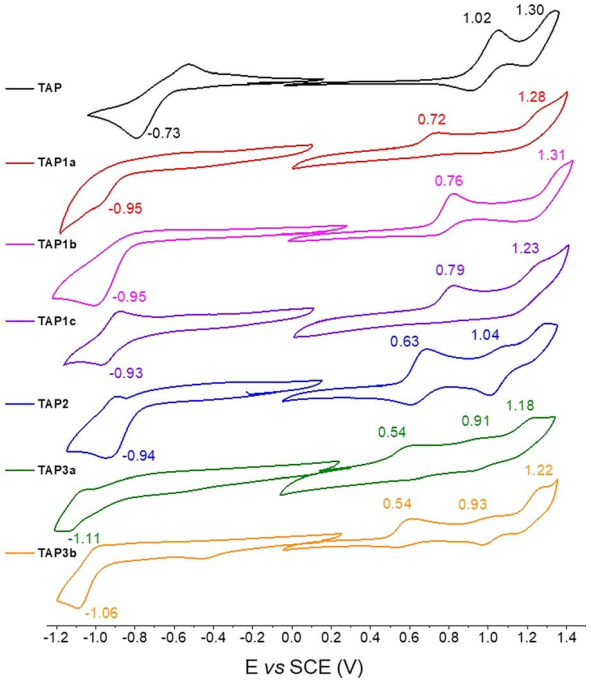

Fig. 3 Cyclic voltammograms of **TAP1–3** recorded in DCM (10^{-3} M) in the presence of tetra-*n*-butylammonium hexafluorophosphate as supporting electrolyte (10^{-1} M), with a scan rate of 100 mV s^{-1}.

into the substituent effect on the redox potential values (Fig. 3). Surprisingly, while the unsubstituted **TAP** presents a reduction process at −0.73 V/SCE, the introduction of electron-withdrawing moieties shifts the reduction potential of the substituted compounds to more negative values *ca.* −0.94 V/SCE, with no significant difference between the four dyes. This observation suggests that the reduction process does not occur at the same site upon introduction of the EWG. For the **TAP3** series, the reduction gets even more cathodically shifted to −1.11 and −1.06 V/SCE respectively, which is explained by the introduction of an additional amine. On the same trend, the first oxidation event becomes easier, shifting from 1.02 V/SCE for the unsubstituted **TAP** to 0.72–0.79 V/SCE for the acylated compounds and 0.63 V/SCE for fluoro-dinitrophenyl bearing **TAP2**. The **TAP3** dyes are prone to oxidation at even lower potentials of 0.54 V/SCE. Overall, the electrochemical gap is being reduced for all the functionalized species **TAP1–3** compared to the unsubstituted congener **TAP**, which is consistent with the recorded optical trend (*vide infra*).

Photophysical properties

Afterwards, we investigated the absorption and emission properties, notably aiming to explore the potential modulation of the optical characteristics of the post-functionalized derivatives, and their consistence with the reduction of the electrochemical gap. Compared to the parent derivative **TAP**, for which the absorption is centered in the green region (λ_{max} = 533 nm, Fig. 4 and Table 1), the acylated dyes **TAP1a–c** all display redshifted absorptions peaking at 606 nm, with a shoulder at 508 nm, and molar extinction coefficients (ε) in the order of 20

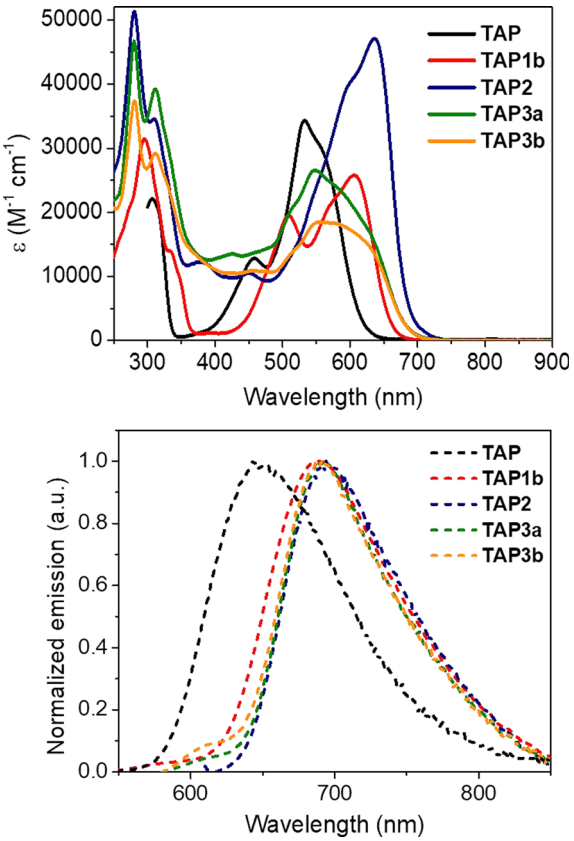

Fig. 4 Electronic absorption and normalized emission spectra of the parent TAP and isolated TAP1b, TAP2 and TAP3a,b dyes in DCM.

000–25 000 M^{-1} cm^{-1} (Table 1, Fig. 4, and S1–S3, ESI†). The trifling differences in absorption maxima for the **TAP1** series points out a negligible effect of the electron-withdrawing amide nature. The EWG effect is more pronounced for the fluorodinitrophenyl substituted **TAP2**, which lowest energy absorption band is peaking at 635 nm with ε = 45 000 M^{-1} cm^{-1} (Table 1, Fig. 4 and S4 in the ESI†). The replacement of the electron-withdrawing fluorine atom with alkyl- or arylamine donors in **TAP3a,b** is accompanied in both cases by a blueshift towards the green region, with maxima found at 548 nm and 552 nm, respectively (, Table 1, Fig. 4, S6 and S7 in the ESI†).

The unsubstituted **TAP** displays a bright emission with a narrow red-located (λ_{em} = 645 nm) fluorescence band (Fig. 4, Table 1). The introduction of electron-withdrawing substituents considerably shifts the emission maxima towards the far-red and even NIR regions. For the acylated **TAP1a**, **TAP1b** and **TAP1c** the band is peaking at 703, 685 and 687 nm (Table 1, Fig. 4, and S1–S3 in the ESI†) with quantum yields of 2.7%, 3.9% and 5.2%, respectively (Table 1), while for **TAP2** we witness a fluorescence band centered at 694 nm and tailing in the NIR region. Upon the modification of the primary amine unit, there is a remarkable increase in the nonradiative deexcitation of all the dyes, from four-fold to twenty-fold, compared to the parent **TAP** (see Table 1), and hence a marked decrease of quantum yield. The different alkyl- or arylamine substituent in **TAP3a,b** has no effect on the emission band (Fig. 4 and Table 1) but an unexpected drop in fluorescence efficiency is noticed for the arylamine functionalized derivative.

The excellent solubility of the isolated phenaziniums allowed to record a solvatochromism study, for which purpose we selected **TAP1b** and **TAP2**. The results highlight a trend of the absorption band to become narrower and accompanied by a moderate bathochromic shift with the increased polarity of the medium, ranging from 594 nm in toluene to 621 nm in MeOH for **TAP1b** and from 592 nm in toluene to 659 nm in DMSO for **TAP2** (Fig. 5). The weak positive solvatochromism is also a feature of the parent compound **TAP**. When the fluorescence of **TAP3a,b** was measured in MeOH and dioxane, a strong redshift was observed in the former solvent (Fig. S8 in the ESI†). This tendency suggests that the solvent-mediated stabilization of the excited-state is higher in protic solvents, leading to redshifted emissions with higher Stokes shifts in methanol of approximately 4400 cm^{-1} *vs.* 2150 cm^{-1} recorded for the reference compound **TAP** (see Table 1 for DCM). The influence of the protic nature of MeOH could not be verified as the compounds **TAP2** and **TAP3a,b** displayed quenched emission in MeCN and DMSO. Compared to the parent **TAP2** derivative, the **TAP3a,b** dyes showed increased values of emission efficiency (Table 1).

The acidochromic properties of the new dyes were shortly investigated as well, knowing the several protonation states reported for **TAP**.[27] Upon addition of trifluoroacetic acid (TFA), the absorption spectra of the **TAP1a–c** series is blueshifted

Table 1 Summary of the optical properties for the isolated TAP1–3 and parent dye TAP

Dye	Solvent	λ_{max} (nm), (ε (M^{-1} cm^{-1}))	λ_{em} (nm)	ΔSS[a] (cm^{-1})	Φ^b	τ (ns)	$k_R{}^c$ (10^6 s^{-1})	$k_{NR}{}^c$ (10^6 s^{-1})
TAP	MeCN[d]	553 (43 140), 465 (16 340)	637	2380	63%	6.6	95	56
	DCM	533 (34 340)	645	3260	69%	6.1	113	50
TAP1a	DCM	606 (19 000), 560 (16 880), 508 (15 200)	703	2280	2.7%	4.2	6.4	231
TAP1b	DCM	606 (25 750), 508 (19 500)	685	1900	3.9%	4.7	8.3	204
TAP1c	DCM	606 (20 260), 569 (18 190), 507 (17 000)	687	1950	5.2%	5.6	9.3	169
TAP2	DCM	635 (45 000), 596 (39 560), 450 (10 500)	694	1340	<1%	1.0	10	990
TAP3a	DCM	548 (26 570)	694	3840	6.3%	3.6	18	260
TAP3b	DCM	552 (18 500)	694	3710	1%	2.6	4	380

[a] ΔSS: Stokes shift, calculated as a difference between the absorption and emission maxima. [b] Relative fluorescence quantum yields measured with oxazine 725 perchlorate as reference (ϕ = 11% in EtOH, λ_{ex} = 620 nm) for **TAP1–3**, or rhodamine B as reference (ϕ = 70% in MeOH, λ_{ex} = 530 nm) for **TAP**. [c] Radiative and non-radiative decay constants calculated using the following equations: $k_R = \phi/\tau$ and $k_{NR} = (1 - \phi)/\tau$. [d] From ref. 27.

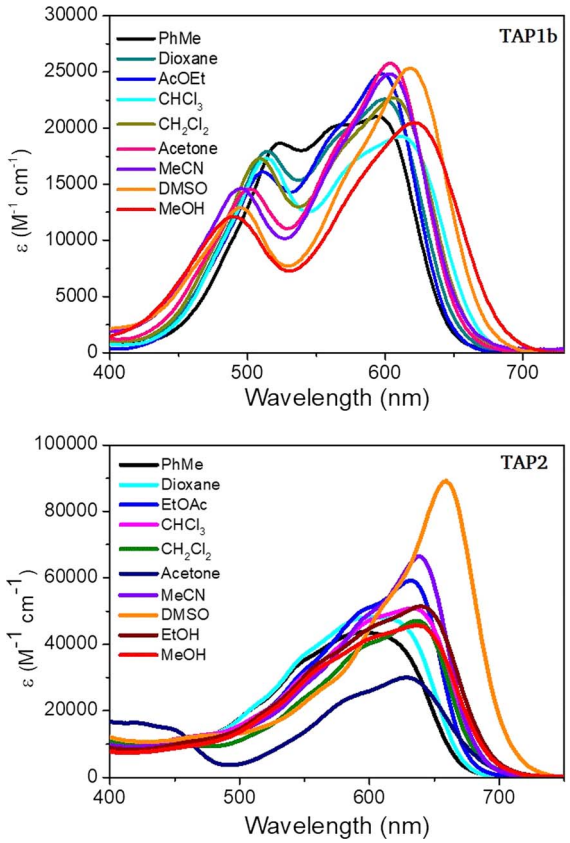

Fig. 5 Electronic absorption solvatochromism of TAP1b and TAP2 ($c = 1.15 \times 10^{-5}$ M and 1.3×10^{-5} M respectively).

towards 519–548 nm (Fig. 6 and S2–S3 in the ESI†). This trend suggests the protonation of the amino-phenazinium, in a similar manner to the parent phenazinium **TAP** and is explained by a rather localized electronic structure. On the emission spectra, this translates into the appearance of a shoulder along with the maintaining of the main emission band, contrary to parent derivative **TAP**, whose protonation induces the loss of emission properties. The addition of 1,8-diazabicyclo[5.4.0]undec-7-ene (DBU) leads to almost negligible hyperchromic and bathochromic absorption shifts, with a trifling hypsochromic effect on the fluorescence spectra. Considering the acidity of the NH proton linked to the acyl group, this outcome might be explained by the possibility that compounds **TAP1a–c** are partially deprotonated in the diluted solutions, DBU addition only increasing the process.

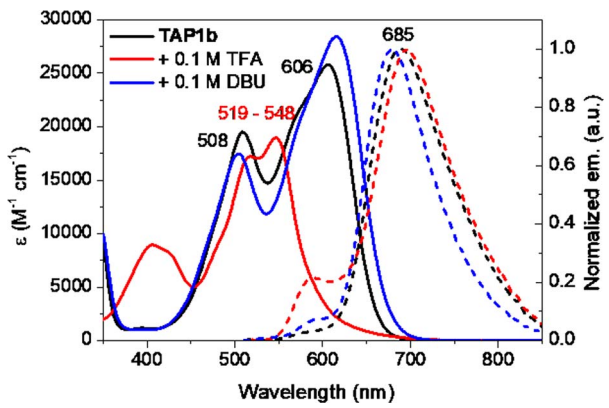

Fig. 6 Electronic absorption (solid lines, $c = 1.15 \times 10^{-5}$ M) and normalized emission (dashed lines) spectra of TAP1b in DCM ($\lambda_{ex} = 510$ nm), DCM + TFA ($\lambda_{ex} = 510$ nm) and DCM + DBU ($\lambda_{ex} = 565$ nm).

As expected, upon introduction of a strong EWG, a high excess of acid is needed to partially protonate **TAP2**, and this event is accompanied by a less intense and blueshifted absorption band as well as a notably blueshifted emission (see Fig. S4†). Addition of DBU induces the appearance of an additional shoulder, while maintaining the main absorption band. The already weak emission of **TAP2** is even more quenched in basic medium. To eliminate the possibility that the compound is already deprotonated in solution (due to water traces), the measurements were repeated in anhydrous DCM, additionally dried over molecular sieves (Fig. S5 in the ESI†). We could witness the same behavior upon the addition of TFA. Basified solution, on the contrary, showed an evolution within 1 hour timeframe, the deprotonated species exhibiting a blue-shifted absorption ($\lambda_{max} = 543$ nm). The transition turned to be reversible upon TFA addition, pointing towards a slow deprotonation process, and therefore ruling out an eventual nucleophilic reaction with DBU.

Finally, the fluorescence lifetime measurements performed on the starting derivative **TAP** and the functionalized series **TAP1–3** return rather long values for NIR emitters, ranging from 1 to 6.6 ns. These results can be easily correlated with the efficiency of the emission process and are explained by the high rigidity of the tricyclic phenazinium core (Table 1 and Fig. S9 in the ESI†).

Theoretical calculations

To obtain additional insights we performed theoretical calculations using TD-DFT and CC2, as detailed in the ESI.† Fig. 7 shows electron density difference (EDD) plots corresponding to the absorption. For **TAP**, one can see alternance of blue (loss of density) and red (gain of density) regions, the two intracyclic nitrogen atoms gaining density whereas the side amino groups lose some density. This alternance is quite typical of a cyanine-like character. This is confirmed by the very small charge-transfer character determined for **TAP** (see Table S1 in the ESI†). Theory foresees a 0–0 energy of 1.97 eV (630 nm, see Table S2 in the ESI†) for **TAP**, which fits quite well the experimental absorption–emission crossing point (2.05 eV, see Fig. S1†). All substituted systems that were modelled, namely **TAP1b**, **TAP2**, **TAP3a** and **TAP3b**, display similar EDD plots, that differ from the one of **TAP** by the significant asymmetry between the contributions of the side amino groups (Fig. 7). In other words, the transition gains a mild yet non-trifling CT character.

This is confirmed by the data of Table S1:† the absorption of **TAP1–3** induces the transfer of *ca.* 0.5 electron over 1.2–1.6 Å. This variation of excited-state nature is accompanied by significant redshifts of the absorption and emissions (Table S2†), which fits the measurements. The two effects (CT

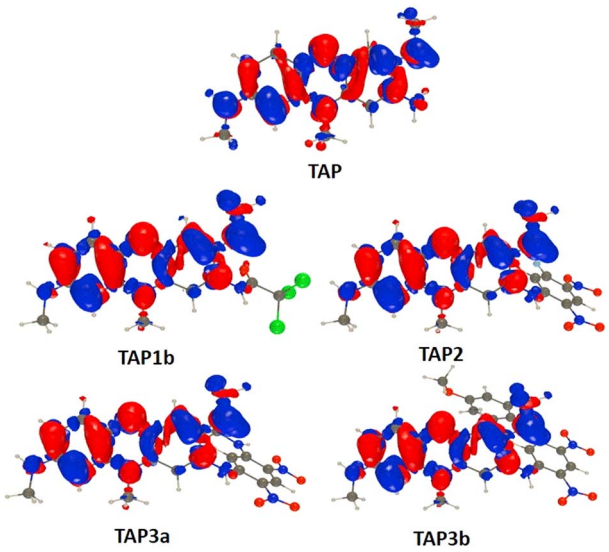

Fig. 7 Electron density difference plots for the lowest excited-state (S_0–S_1) of the investigated compounds. The red and blue lobes correspond to regions of increase and decrease of density upon absorption. Contour threshold: 0.001 au.

character and redshift), naturally explain the drop in fluorescence quantum yield from **TAP** to **TAP1–3**. One aspect that remains intriguing however is the strong difference of quantum yield between **TAP3a** and **TAP3b**, despite very similar spectral properties. In **TPA3a**, the computed TD-DFT S_0–S_1 absorption is bright and mainly corresponds to a HOMO–LUMO excitation, both orbitals being mainly centered on the phenazium core, *i.e.*, the expected trend is obtained. In contrast, in **TAP3b**, the computed TD-DFT S_0–S_1 excitation can be mainly ascribed to a HOMO-1 to LUMO transition, the HOMO being localized on the side group (see the ESI† for details). On can therefore suspect the presence of photoinduced electron transfer in **TAP3b**.

Conclusions

In conclusion, we have investigated the straightforward post-functionalization of a triamino-phenazinium dye **TAP** and showed that the introduction of electron-withdrawing groups on the reactive primary amine function has a dramatic impact on the electron density of the phenazinium core (**TAP1–3**). The synthetic approach, employing a one-step acylation or nucleophilic aromatic substitution, induces a drastic colour change and enables the easy access to dyes with red to far-red absorption and NIR emission properties, making them attractive candidates for biological staining and therapeutic applications. Notably, the **TAP2** derivative, bearing a reactive fluorine moiety holds promise as a versatile platform for substitution reactions with nucleophiles and easy bioconjugations with drugs, sugars or proteins. Alternatively, the incorporation of fluorine moieties can enhance the pharmacokinetic profile and staining capacities of fluorophores. Moreover, an advantageous combination of complementary fluorescence imaging and PET (positron emission tomography) scan technique, for example, open the possibility for a superior resolution imaging probe, especially for the oncology field.

Author contributions

S. P. and O. S. conceived, designed and supervised the project. T. M., J.-F. L. and G. C. designed and conducted the experiments and collected and analysed the results. D. J. performed and analyzed the theoretical calculations. T. M. and S. P. drafted the manuscript. All authors read, reviewed, and approved the final draft.

Conflicts of interest

There are no conflicts to declare.

Acknowledgements

O. S. acknowledges the financial support of CNRS Innovation for the prematuration program (grant of J.-F. L.), and the Ministère de la Recherche et de l'Enseignement supérieur (T. M. grant). S. P. acknowledges the financial support of the Agence Nationale de la Recherche, in the frame of the SOCOOL project (ANR-20-CE07-0024). O. S. thanks the Spectropole (Aix-Marseille Univ.) for X-ray diffraction study and HRMS analyses. D. J. is indebted to the GliCID mesocenter for computational resources.

References

1 W. H. Perkin, *J. Chem. Soc. Trans.*, 1896, **69**, 596–637.
2 H. Berneth, in *Ullmann's Encyclopedia of Industrial Chemistry*, Wiley, 1st edn, 2008.
3 N. Hughes, in *Rodd's Chemistry of Carbon Compounds*, ed. S. Coffey, Elsevier, Amsterdam, 2nd edn, 1964, pp. 403–436.
4 J. Yan, W. Liu, J. Cai, Y. Wang, D. Li, H. Hua and H. Cao, *Mar. Drugs*, 2021, **19**, 610, DOI: **10.3390/md19110610**.
5 J. B. Laursen and J. Nielsen, *Chem. Rev.*, 2004, **104**, 1663–1686.
6 A. Cimmino, A. Evidente, V. Mathieu, A. Andolfi, F. Lefranc, A. Kornienko and R. Kiss, *Nat. Prod. Rep.*, 2012, **29**, 487–501.
7 E. Bindewald, R. Lorenz, O. Hübner, D. Brox, D.-P. Herten, E. Kaifer and H.-J. Himmel, *Dalton Trans.*, 2015, **44**, 3467–3485.
8 B. Liu, K. Liu, Y. Lu, D. Zhang, T. Yang, X. Li, C. Ma, M. Zheng, B. Wang, G. Zhang, F. Wang, Z. Ma, C. Li, H. Huang and D. Yin, *Molecules*, 2012, **17**, 4545–4559.
9 M. Pieroni, in *Annual Reports in Medicinal Chemistry*, Elsevier, 2019, vol. 52, pp. 27–69.
10 D. Zhang, Y. Lu, K. Liu, B. Liu, J. Wang, G. Zhang, H. Zhang, Y. Liu, B. Wang, M. Zheng, L. Fu, Y. Hou, N. Gong, Y. Lv, C. Li, C. B. Cooper, A. M. Upton, D. Yin, Z. Ma and H. Huang, *J. Med. Chem.*, 2012, **55**, 8409–8417.
11 L. Benoit and S. T. Cole, *Antimicrob. Agents Chemother.*, 2015, **59**, 4457–4463.
12 S. Dadras, E. Mohajerani, F. Eftekhar and M. Hosseini, *Curr. Microbiol.*, 2006, **53**, 282–286.

13 A. C. Voos, S. Kranz, S. Tonndorf-Martini, A. Voelpel, H. Sigusch, H. Staudte, V. Albrecht and B. W. Sigusch, *Laser Surg. Med.*, 2014, **46**, 235–243.
14 R. Combuca da Silva Junior, K. da Silva Souza Campanholi, F. dos S. Rando, R. S. Gonçalves, D. Lazarin-Bidóia, F. A. Pedroso de Morais, A. P. Alves dos Santos Silva, C. V. Nakamura, M. Soares dos Santos Pozza and W. Caetano, *Dyes Pigments*, 2022, **197**, 109900.
15 H. Babich and E. Borenfreund, *Altern. Lab. Anim.*, 1990, **18**, 129–144.
16 G. Repetto, A. del Peso and J. L. Zurita, *Nat. Protoc.*, 2008, **3**, 1125–1131.
17 J. F. Riley, *Cancer Res.*, 1948, **8**, 183–188.
18 H. Endo and M. Tada, *Sci. rep. Res. Inst., Tohoku Univ., Ser. C*, 1965, **12**, 53–57.
19 G. Hong, A. L. Antaris and H. Dai, *Nat. Biomed. Eng.*, 2017, **1**, 0010.
20 Y. Jiang and K. Pu, *Adv. Biosyst.*, 2018, **2**, 1700262.
21 S. Pascal, S. David, C. Andraud and O. Maury, *Chem. Soc. Rev.*, 2021, **50**, 6613–6658.
22 A. Tsuda and A. Osuka, *Science*, 2001, **293**, 79–82.
23 X.-D. Jiang, R. Gao, Y. Yue, G.-T. Sun and W. Zhao, *Org. Biomol. Chem.*, 2012, **10**, 6861–6865.
24 A. Loudet, R. Bandichhor, K. Burgess, A. Palma, S. O. McDonnell, M. J. Hall and D. F. O'Shea, *Org. Lett.*, 2008, **10**, 4771–4774.
25 L. Chen, C. Li and K. Müllen, *J. Mater. Chem. C*, 2014, **2**, 1938–1956.
26 D. F. Gloster, L. Cincotta and J. W. Foley, *J. Heterocycl. Chem.*, 1999, **36**, 25–32.
27 Z. Chen, S. Pascal, M. Daurat, L. Lichon, C. Nguyen, A. Godefroy, D. Durand, L. M. A. Ali, N. Bettache, M. Gary-Bobo, P. Arnoux, J.-F. Longevial, A. D'Aléo, G. Marchand, D. Jacquemin and O. Siri, *ACS Appl. Mater. Interfaces*, 2021, **13**, 30337–30349.
28 S. Golovynskyi, I. Golovynska, L. I. Stepanova, O. I. Datsenko, L. Liu, J. Qu and T. Y. Ohulchanskyy, *J. Biophot.*, 2018, **11**, e201800141.